Real-time dynamics of clusters. I. I_2X_n ($n=1$)

D. M. Willberg, M. Gutmann,[a] J. J. Breen,[b] and A. H. Zewail
Arthur Amos Noyes Laboratory of Chemical Physics, California Institute of Technology, Pasadena, California 91125

(Received 16 August 1991; accepted 19 September 1991)

Vibrational predissociation of I_2X_n (X = Ne, Ar) van der Waals clusters are studied in real-time using picosecond pump–probe (LIF) and molecular beam techniques. The state-to-state rates of vibrational predissociation are measured for specific vibrational levels v_i' by monitoring the rise of nascent I_2. Here, we report our study of

$$I_2X(B,v_i') \xrightarrow{k(v_i',v_f')} I_2(B,v_f') + X.$$

For I_2Ne, the values of $\tau = k^{-1}(v_i',v_f')$ decrease nonlinearly from 216 ps for $v_i' = 13$ to 53 ps for $v_i' = 23$. For I_2Ar (B,v_i'), which undergo electronic and vibrational predissociation, the risetime of the nascent I_2 is found to be 70 ps when $v_i' = 18$ and 77 ps when $v_i' = 21$. A number of theoretical models for vibrational predissociation (the energy-gap law, the momentum-gap law, quantum and classical calculations) are compared with our experimental results in an attempt to understand the key features of the dynamics and the potential energy surface.

I. INTRODUCTION

Besides yielding important information on "static" intermolecular interactions (for reviews see Refs. 1, 2), van der Waals clusters are challenging and "simple" systems for understanding reaction dynamics. Of great interest are the questions pertaining to energy redistribution and fragmentation and their dependence on cluster size. It is not obvious that the clusters will be the intermediates between gas-phase and liquid-phase limits of dynamics, but their finite size offers a unique opportunity for testing microscopic and macroscopic theories.

Real-time studies of large vdW complexes have been reported for isoquinoline,[3] tetrazine (in S_1 and S_0),[4,5] phenol,[3] cresol,[3] perylene,[6] stilbene,[3,7] aniline,[8] and $(NO)_2$ (in S_0),[9] and recently results have become available for the family of halogens. With nanosecond lasers, the lifetime of ICl–Ne in its A state was measured to be 3 ± 2 ns for $v' = 14$ by the Lester group,[10] and for a large number of systems linewidth measurements have been used to deduce vibrational predissociation lifetimes (for recent reviews see Refs. 11–13).

Even in small clusters there remain unanswered questions, especially when one is interested in relating the dynamics to the forces governed by the potential. For example, as discussed below, the dynamics of I_2Ne show the predissociative nature of the cluster (in its B state) while those of I_2Ar indicate the presence of electronic predissociation, i.e., the breakage of the I–I bond in the presence of Ar. One may ask: Does the repulsive force of the van der Waals bond determine the state-to-state rates of predissociation? Do vibrational and electronic predissociations have the same origin? These are two of the many questions that one would like to address in the so-called simple I_2X_n systems.

In the real-time picture, the time scales for the different motions and interactions are relevant to the dynamics. The vibrational period (τ_v) of the I_2 wave packet in the B state is typically 300 fs in the region of interest here.[14] The available energy for a change of one quantum in the I_2 vibration, between the initial and final states of the I_2Ne system ($v_i' = 19$, $v_f' = 18$), translates to a typical velocity of about 130 m/s. With a repulsive distance scale of $L \sim 0.5$ Å one obtains a "half-collision" time $t_c \sim 380$ fs. The ratio of t_c/τ_v reflects the adiabaticity of the half-collision, and L plays an important role in the outcome of I_2 energy relaxation. As t_c decreases, the (nonadiabatic) energy transfer becomes more efficient since the change of force is large during this short time. The state-to-state rates are characterized by times much longer than t_c and τ_v.

This paper gives a fuller account of an earlier communication[15] which reported our first study of the small clusters of iodine/rare gas systems in real-time. When there is only one rare gas atom, I_2X (X = Ne,Ar), the focus is on the problem of intramolecular vibrational-energy redistribution (IVR), vibrational predissociation (VP), and their relationship to the nature of the binding van der Waals potential. In a separate paper,[16] we present our findings for I_2X_n ($n > 1$).

These small clusters are ideal for studies of VP and IVR for a number of reasons. First, the vibrational dynamics (the I_2 stretch, the van der Waals stretching mode, and the van der Waals bending mode) are well defined. As this is a relatively simple system, there are a variety of theoretical models (quantum and classical) which may be formulated and tested with the experimental results. Second, elegant and comprehensive spectroscopic studies are available on these systems.[17–23] Third, the I_2 real-time dynamics on the femtosecond–picosecond time scales have already been reported.[14] Finally, unlike the case of large molecules, theory is quite advanced for these smaller systems (*vide infra*), and there is hope for detailed understanding of IVR and VP.

Frequency-domain spectroscopic studies of I_2X_n

[a] Deutsche Forschungsgemeinschaft post-doctoral fellow from Germany,
[b] Present address: Department of Chemistry, Columbia University, Havemeyer Hall, New York, NY 10027.

 0021-9606/92/010198-15$06.00

(where X = He, Ne, and Ar; $n \geqslant 1$) give the spectral shift of the $B \leftarrow X$ transition of I_2X to be 6.65 cm^{-1} for neon, and 13.26 cm^{-1} for argon[17] (note that this shift varies slightly with v'). The state-to-state channels by which VP occurs have also been determined.[18–20] The primary channel for I_2Ne is given in Eq. (1):

$$I_2Ne^*(v_i') \xrightarrow{k(v_i',v_f')} I_2^*(v_f' = v_i' - 1) + Ne, \quad (1)$$

where the asterisk denotes the electronically excited B state. The situation for I_2Ar is different due to the presence of both electronic and vibrational predissociation channels, as discussed below. By performing channel closing experiments—determining at which values of v_i' various channels were opened or closed—Levy and co-workers were also able to obtain the van der Waals bond energies of the different clusters.[21]

The first step in Eq. (1) is the absorption of a photon which prepares the cluster in a well-defined vibrational level v_i' of the I_2 stretching mode. This is followed by energy redistribution from this mode into the van der Waals stretching mode. In the case of neon, the energy of one quantum of the I_2 stretching mode exceeds the van der Waals binding energy of the complex. Therefore, energy redistribution results in fragmentation, with I_2 being in its B $(v_i' - 1)$ vibronic state, and the excess energy converting into translational kinetic energy and rotational energy of the nascent I_2. Figure 1 shows this process schematically. The theoretical models, which assume an exponential-type repulsion at short I_2–X separations and R^{-6} interactions at long range, predict that the coupling of the I_2 vibrations to the van der Waals stretch coordinate is highly dependent on the initial value for v_i'. As the VP state-to-state rate is directly determined by this coupling, the rates are highly dependent on v_i'.

In order to understand the coupling involved in VP, it is necessary to accurately determine the rates of VP as a function of the initial quantum number v_i'. Levy and co-workers have estimated the VP lifetimes from linewidth measurements.[19,22] Linewidth measurements provide an upper limit for the rate of VP as they are often contaminated by unresolved substructure (only with I_2He are the rotational bands resolved[23]). One may deduce the lifetimes, in the absence of pure dephasing processes, if the transition is homogeneously broadened,[24,25] but homogeneous broadening reflects only the initial step of the dynamics. To observe VP, the state-to-state rates must be measured.

The real-time measurements presented here for I_2Ne and I_2Ar are compared with different theoretical models to test their predictions of the absolute magnitudes of the state-to-state rates and their dependence on energy and the quantum state excited. For I_2Ne the measurements are made over the range $v_i' = 13$ to $v_i' = 23$ and the rates range from $4.6 \times 10^9\ s^{-1}$ to $1.89 \times 10^{10}\ s^{-1}$. For I_2Ar the total rates are $1.30 \times 10^{10}\ s^{-1}$ $(v_i' = 21)$ and $1.43 \times 10^{10}\ s^{-1}$ $(v_i' = 18)$, and the electronic predissociation rate is comparable to the VP rate.

This paper is outlined as follows: In Sec. II the pump–probe scheme and the experimental apparatus are described in detail. We present our results in Sec. III and discuss them in conjunction with the relevant spectroscopy and the different theoretical models. In Sec. IV we give an account of our studies of the I_2Ar system, and we conclude the paper in Sec. V.

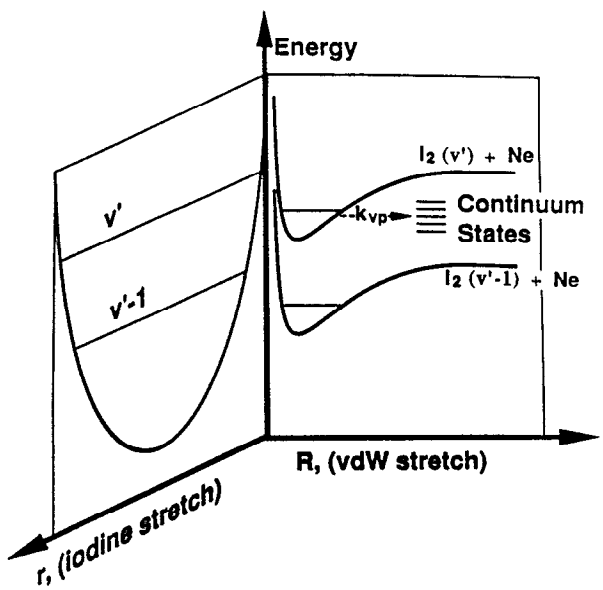

FIG. 1. A schematic of the vibrational predissociation process in a two coordinate space. Shown on the right is the van der Waals stretch coordinate (R) and on the left the I_2 stretch coordinate (r). The I_2 energy levels correspond to an infinite I_2–Ne separation. Vibrational predissociation, a bound to a continuum transition, occurs as one quantum of energy is lost from the I_2 stretch to the van der Waals coordinate.

II. EXPERIMENT

The experiments were performed using a combination of picosecond laser and molecular beam techniques. In this section the experimental methodology will be given, followed by a detailed description of the apparatus.

To measure the state-to-state VP rates as a function of the vibrational quantum number v_i', two color (pump–probe) laser pulses were employed (Fig. 2). The first laser pulse (the pump) excited the iodine to a given v_i' of the B electronic state,[26] covering the range $v_i' = 13$–23. The second laser pulse (probe), which was delayed in time from the first, was tuned to the $F \leftarrow B$ transition of the nascent I_2^* produced by predissociation. Ultraviolet fluorescence from the I_2 F ion-pair state was measured as a function of the delay time between the pump and probe laser pulses. As the delay was varied, the resulting transient yielded the risetime of the nascent $I_2^*(v_f' = v_i' - 1)$. Temporal resolution in experiments of this nature is limited only by the cross correlation of the pump and probe laser pulses.[3] The laser system used in these experiments had a cross-correlation (FWHM) of 40 ± 3 ps, with an approximately Gaussian profile.

The I_2Ne complexes studied were formed in a free jet expansion of neon (99.996% purity, Spectra Gases Inc.) which had been seeded with iodine (99.999% purity, Aldrich) at room temperature vapor pressure. Since the expan-

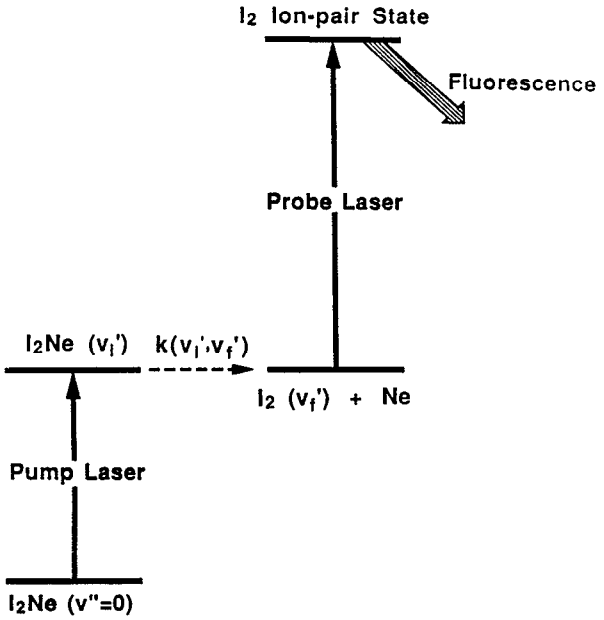

FIG. 2. Diagram showing the experimental scheme used in measuring the state-to-state rates. The pump laser prepares the metastable cluster in a selected vibronic state which then undergoes vibrational predissociation [rate $k(v_i',v_f')$]. The probe laser then excites the nascent I_2^* to an ion-pair state from which UV fluorescence is detected. Transients are obtained by varying the temporal delay between the pump and probe laser pulses.

sion contained both bare iodine and larger complexes of I_2Ne_n (where $n>1$), as well as I_2Ne, selective excitation of the desired complex was important. The spectroscopic measurements published by Levy and co-workers proved invaluable in this regard. It was shown that for the I_2Ne_n complexes, where $n<7$, the $(B,v')\leftarrow(X,v''=0)$ transition is blue shifted ($n\times 6.65$ cm^{-1}) from the corresponding bare I_2 transition.[17] The lasers used in our experiments had a bandwidth of 3 cm^{-1}, and it was possible to selectively excite a given cluster size.

The experimental scheme for the I_2Ar studies was essentially the same as described for I_2Ne, and has been described briefly in an earlier communication.[15] The conditions were as follows. An approximately 20% mixture of Ar in He was seeded with iodine (99.999% purity, Aldrich) at its room temperature vapor pressure. The mixture was expanded through a heated (43 °C) continuous glass nozzle ($d=75\,\mu$m). The backing pressure was typically 20 psi, and x/d was kept at about 75.

A number of test experiments were performed. First, prior to each I_2Ne (v_i') scan, an I_2 ($v_i'-1$) scan was taken. In the latter the pump laser was tuned to the uncomplexed B $(v_i'-1)\leftarrow X$ $(v''=0)$ transition, while the probe laser was set for the same transition used in the I_2Ne scan. As in the I_2Ar cluster $v_f'=v_i'-3$, a corresponding I_2 $(v_i'-3)$ scan was made for this system. These tests ensured the correct probe laser wavelength, as well as proper alignment between the pump and probe lasers. Second, UV fluorescence was shown to decrease as the pump laser was detuned either to the red or to the blue of the I_2X (X = Ne,Ar) absorption maximum, indicating that the signal was not due to the "tail" of a bare iodine transition. Third, the molecular beam conditions were varied: signal intensity was found to be highly dependent on the stagnation pressure behind the nozzle (as expected for van der Waals clusters), and no signal was observed when pure helium was used as the carrier gas. Finally, multiple transients were obtained for each vibrational level to ensure the accuracy of the measurements.

A. Molecular beam apparatus

The molecular beam apparatus, which was built specifically for studying gas phase clusters,[27] is schematically presented in Fig. 3. The beam apparatus consisted of three chambers: the source, buffer, and time-of-flight (TOF) compartment. The source chamber was pumped by a Varian VHS-10 diffusion pump, while the buffer and TOF chambers were each pumped by Varian VHS-6 diffusion pumps. The VHS-10 diffusion pump was backed by a Leybold–Heraeus D90A mechanical pump, while the other two diffusion pumps were backed by a Leybold–Heraeus D60A.

The nozzle was mounted on a carriage which can be translated along the molecular beam axis. This design allowed for adjustment of the x/d ratio. Two different nozzles were used, a cw glass nozzle for I_2Ne $v_i'=16-21$, and a General Valve series 9 pulsed solenoid valve for $v_i'=13,14,22,23$. The glass nozzle was home-built and had an orifice diameter of 75 μm. The nozzle was heated to 43 °C to avoid clogging with I_2. The pulsed nozzle had a conical cross section for maximum cluster formation, with a nozzle diameter of 150 μm. The pulsed nozzle was not actively heated during the experiments performed in the studies reported

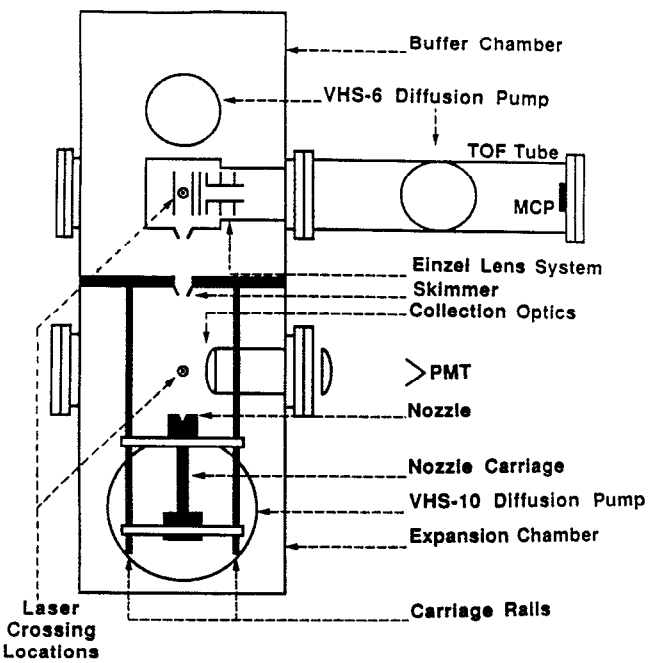

FIG. 3. Schematic of the molecular beam apparatus used in these studies. Details about the system are given in the text. PMT stands for photomultiplier tube, MCP for multichannel plate, and TOF for time-of-flight.

here, however, as it was operated, it reached an equilibrium temperature of approximately 45 °C. The cw nozzle made it possible to perform the experiments at the maximum Q-switching repetition rate of the laser (typically 800 Hz); the backing pressure was limited to 40 psi with pure neon. For the pulsed nozzle experiments, although the repetition rate was limited to 100–130 Hz, a backing pressure of at least 130 psi with pure neon was obtained.

B. Laser system

The picosecond laser system is schematically shown in Fig. 4. The essential design[28(a)] consisted of a mode-locked, Q-switched, frequency-doubled Nd:YAG laser which synchronously pumped two cavity-dumped dye lasers. The Nd:YAG was home-built with components from a Quantronix 416 laser. The laser was mode-locked at 76 MHz, and could be operated at various Q-switching repetition rates, typically at 800 Hz when the cw nozzle was used in the molecular beam, and at 100 Hz for use with the pulsed nozzle. A KTP crystal was used to frequency double the 1.06 μm output of the Nd:YAG laser, with a produced energy of 800 μJ per Q-switched pulse envelope at 532 nm. The temporal width of a mode-locked pulse within the Q-switched pulse envelope was measured to be approximately 100 ps.

The 532 nm output of the Nd:YAG laser was split to synchronously pump the two cavity dumped, etalon tuned dye lasers which are operated in tandem. The dye lasers are home-built.[27] Briefly, the dye laser cavity was defined by two planar broadband high reflecting mirrors; a 25 cm plano-convex lens was used as the focusing element within the cavity. A flowing dye cell (thickness: 1 mm) was located as close to one of the mirrors as possible, and was also at the focal point of the lens. The cavity dumper consisted of a Pockels' cell operated at its quarter-wave-plate voltage, coupled with a Glan laser prism.[28(b)] Leakage of 1.06 μm light through the high reflector of the Nd:YAG laser was detected by a fast photodiode (EG&G FND-100); this signal was sent to a digital delay generator, which then triggered the Pockels' cell.

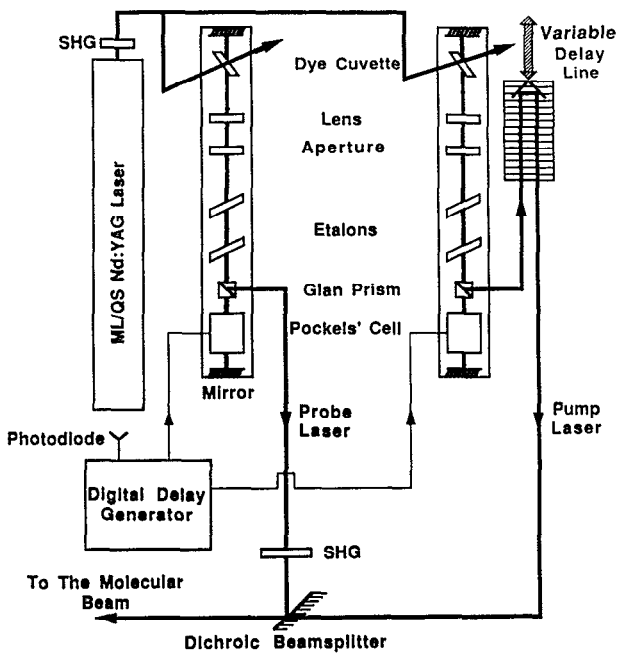

FIG. 4. Schematic of the two color pump–probe picosecond laser system. Details of the system are given in the text. SHG stands for second harmonic generation.

Two intracavity etalons (a 5 μm airgap and a 100 μm solid etalon) were used for wavelength selection. For the majority of the vibrational states studied, dye solutions of rhodamine 590 (Exciton) in methanol were used for the pump laser, and DCM (Exciton and Kodak) in DMSO was used for the probe laser. For the vibrational states $v_i' = 13,14$, rhodamine 610 (Exciton) in methanol was used for the pump laser. The visible light from the probe laser was frequency doubled to the UV with a KDP crystal phase matched for 600 nm.

The energy of the pump laser pulse was $\sim 5\ \mu$J and that of the frequency-doubled probe pulse was $\sim 0.2\ \mu$J. The bandwidths of both lasers (close to Gaussian in profile) had FWHM of 3 cm^{-1}, as measured on a Spex half-meter monochromator. Special care was taken in the adjustment of the etalons to prevent sidebands from interfering in the experiments.

The cross correlations of the pump and probe lasers were measured at each of the wavelength combinations used in these experiments. They typically were Gaussian in profile with a FWHM value of 40 ± 3 ps, and did not vary significantly over the entire range of wavelength combinations used. The cross correlations were measured without the KDP frequency doubler in place after the probe laser, and thus the cross correlation was that of the visible pump and probe lasers.

The variable temporal delay between the pump and probe lasers was achieved by using two optical delay lines. The output of the probe laser was passed through a constant delay line after the frequency doubling. The output of the pump laser was collimated and sent to a Michelson interferometer type delay line which was operated by a linear positioning stage (Aerotech ATS224) driven by a stepper motor. This stage had a spatial resolution of 1 μm/step, which was much higher than was required. Typically, we used 500 steps per data point which corresponded to a temporal delay of 3.3 ps. The pump and probe beams were spatially overlapped on a dichroic beamsplitter and, after being gently focused (100 cm lens), they crossed the supersonic beam perpendicularly. When the cw nozzle was used, the lasers intersected the molecular beam 6 mm downstream from the nozzle ($x/d = 75$); with the pulsed nozzle, the laser crossed 25 mm downstream ($x/d = 70$).

Fluorescence was collected, passed through an UG-11 filter to reject scattered visible light, and imaged onto a photomultiplier tube. The signal was amplified 25× by a preamplifier (Stanford Research Systems, SRS445), and was integrated over a number of laser shots on a boxcar averager (Stanford SRS250). The integrated signal at different delays was processed via an analog-to-digital board and stored in an Apple MacIntosh II microcomputer.

III. RESULTS AND DISCUSSION

A. State-to-state rates

Figure 5 shows transients for three of the vibrational quantum numbers, $v_i' = 13,18$, and 23, studied. The time constants (τ) were extracted from the transients by fitting them to an exponential rise, including a convolution with the Gaussian system response function. The fitting procedure was based on a Marquardt nonlinear least-squares fitting routine.[29] For all transients reported, no parameters were fixed other than the cross-correlation bandwidth. The value of time zero obtained from these transients corresponded well to that obtained from bare I_2 control scans; there was no evidence of an induction period in the case of I_2Ne, within our time resolution. The measured τ, as a function of v_i', are shown in Fig. 6 and are listed in Table I. Note that the errors listed are the standard deviations of all values obtained for a given v_i'.

An interesting feature that we have observed in the $v_i' = 22$–23 transients was the appearance of rotational recurrences corresponding to nascent $I_2^*(v_i' - 1)$, as can be seen in Fig. 7. For all of the transients measured, the pump and probe lasers had parallel polarizations and the rotational recurrences observed were found to be in accord with this arrangement. When I_2Ne was pumped to $v_i' = 23$ and the product I_2^* was probed in $v_f' = 22$ the spacing between the in-phase and out-of-phase recurrences was found to be 336 ± 5 ps. This corresponds to a rotational constant of 0.024 83 cm^{-1}, which is in good agreement with the literature value of 0.024 85 cm^{-1} for I_2 in the $v' = 22$ vibronic state.

For these values of v_i', the process of VP is relatively fast so that rotational coherence of the sampled population is preserved. This is an important result when considering the effect of rotations on VP. At the rotational temperature of the beam ($\sim$4–5 K), a number of rotational levels, in any given vibronic state, is excited. Most theoretical models neglect the role of rotationally excited states on the rate of predissociation. The observed rotational recurrences indicate that there is a separation between the timescales of VP and of the rotational motion.

As mentioned above, Levy and co-workers have estimated the predissociation lifetime of I_2Ne in various vibrational levels from linewidth measurements.[19] Their reported estimates, along with the τ values measured in the real-time experiments, are shown in Fig. 8. The value obtained by linewidth measurement for $v_i' = 14$ is significantly shorter then the value obtained in our experiment. As has been previously noted,[19] linewidth measurements of I_2X systems are difficult to unravel due to inhomogeneous broadenings; the rotational congestion is one contribution. The linewidth estimate of τ, therefore, represents an upper limit for the corresponding rate, and this is a possible reason for the differences between Levy's results and ours. The reported errors for the linewidth estimates are large, and it is difficult to establish in this case the functional form for the v' dependence of VP. The values obtained in real time have errors typically less than ten percent of the magnitude of τ, and they show clearly that the v_i' dependence is monotonic, but highly nonlinear, over the range of v_i' measured.

The rate of vibrational predissociation $k(v_i', v_f')$ in Eq. (1) is taken as the inverse of the measured τ. The obtained rates are listed in Table I, and the v' dependence of the rates is shown in Fig. 9. The available energy for the predissociation process in Eq. (1) is defined here as the energy released from one quantum of the I_2 vibrational stretch. Due to the anharmonicity of the I_2 B-electronic state potential surface, the

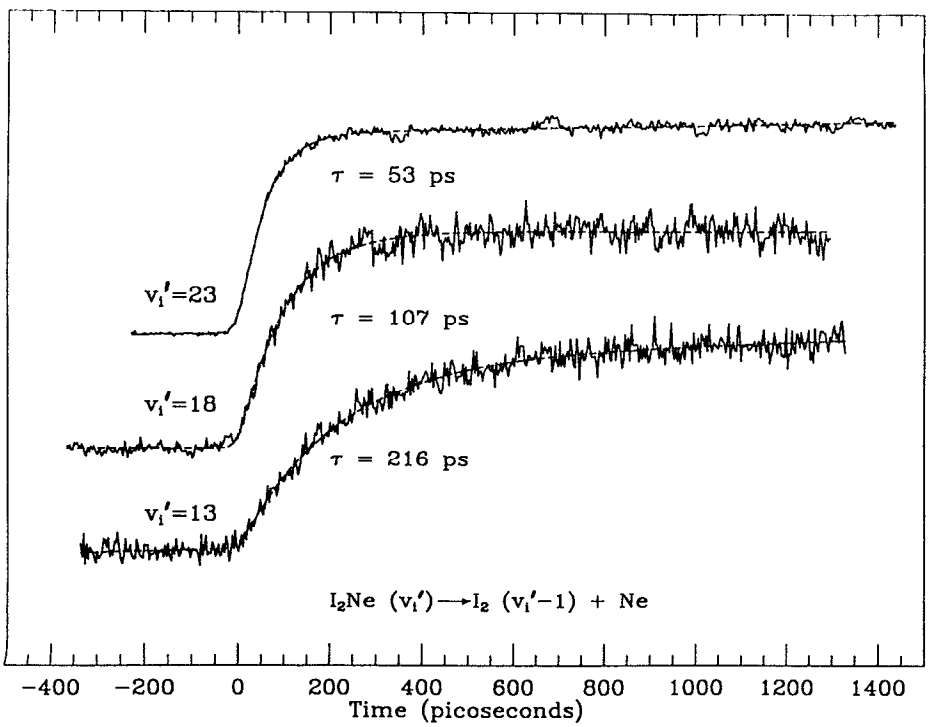

FIG. 5. Representative transients obtained, using the pump–probe scheme described in the text, for three different values of v_i': $v_i' = 13$, 18, and 23. The dashed line is the fit to an exponential rise function, from which the value of the state-to-state rate is given.

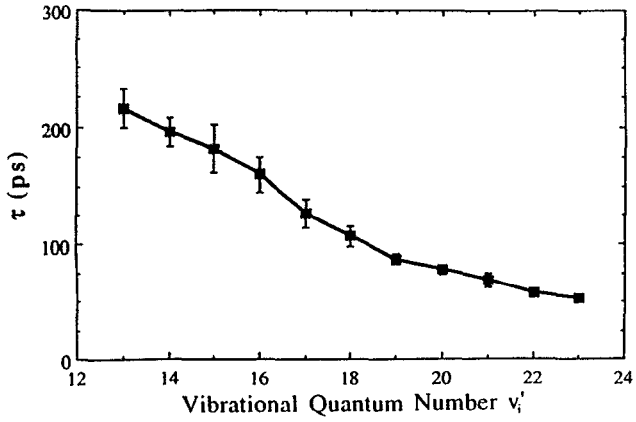

FIG. 6. The vibrational predissociation lifetimes as a function of the initially prepared v_i' state. These values are given in Table I.

energy available for predissociation decreases as v_i' increases. As can be seen in Fig. 10, the rate of predissociation is inversely proportional to the available energy. More on these findings will be discussed in the following section.

B. Comparison with theory

The VP of van der Waals complexes consisting of a diatomic molecule B–C and a rare gas atom X has been the subject of many theoretical studies during the last decade.[30–55] Realizing the fact that VP can be described as a half-collision process, the advanced methodology of scattering theory can be applied, as has been done by Beswick, Jortner (BJ) and co-workers.[30–33] Their treatment of VP essentially considers the decay of a bound complex state into a set of coupled translational continua.

The relevant coordinates for a description of VP are the intramolecular coordinate r of the diatomic fragment and the intermolecular coordinate R (the distance between the rare gas atom X and the center of mass of the B–C molecule, frozen in its equilibrium distance r_0). If rotational and bending motions are considered, the angle θ between these coordinates has to be varied as well.

TABLE I. The state-to-state rates and lifetimes as a function of v_i'.

v_i'	τ (ps)[a]	$k(v_i',v_f')\times 10^9\ s^{-1}$
13	216 ± 16	4.6 ± 0.4
14	196 ± 12	5.1 ± 0.3
15	182 ± 20	5.5 ± 0.6
16	160 ± 15	6.3 ± 0.6
17	126 ± 12	7.9 ± 0.8
18	107 ± 9	9.3 ± 0.9
19	87 ± 4	11.5 ± 0.9
20	78 ± 4	12.8 ± 1.0
21	69 ± 6	14.5 ± 0.7
22	58 ± 3	17.2 ± 0.9
23	53 ± 3	18.9 ± 1.0

[a] The values reported are typically the average of at least five or six independent measurements. The errors are one standard deviation.

The coupling of the vibrations along these coordinates is given by $V(r,R)$, and the full van der Waals potential $U(r,R)$ can be written as:

$$U(r,R) = U(r_0,R) + V(r,R). \tag{2}$$

With this separation, the zero-order Hamiltonian gives a separable basis set; the diabatic bound states in this frozen approximation are direct products $|v_i'\rangle|l'\rangle = |v_i'l'\rangle$, where v_i' labels the quantum state of the oscillation along r [with energy $E_{BC}(v_i')$] and l' that of the vibration along R (with energy $\epsilon_{l'}$). The diabatic continuum states are direct products $|v_f'\rangle|\epsilon'\rangle = |v_f'\epsilon'\rangle$, where ϵ' denotes the energy-normalized continuum state describing the fragments B–C and X flying apart with relative kinetic energy ϵ'. The corresponding energies are $E_{BC}(v_i') + \epsilon_{l'}$ for the bound states and $E_{BC}(v_f') + \epsilon'$ for the continuum states.

Assuming that only the discrete states of the electronic B state are connected to the ground state of the molecule by a nonvanishing optical transition moment, the initial state at time zero can be assumed to be prepared in $|v_i'l'\rangle$. This initial state decays into the continuum exponentially with a lifetime:

$$\tau = (\hbar/2\Gamma); \quad \tau^{-1} = k(v_i',v_f'). \tag{3}$$

As VP of the systems considered here is much faster than the radiative decay, Γ (in energy units) is the HWHM of the dissociation resonance.

By neglecting both the discrete–discrete state and continuum–continuum state coupling, and by assuming that the residual coupling is small compared with the energy spacing between the discrete levels (i.e., neglecting interference effects between resonances), BJ arrived at the golden rule expression:[30]

$$\Gamma = \pi|\langle v_i'l'|V|v_f'\epsilon'\rangle|^2, \tag{4}$$

describing VP into the channel $|v_f'\epsilon'\rangle$. Neglecting the usually small level shifts introduced by the coupling operator, energy conservation implies:

$$\epsilon' = E_{BC}(v_i') + \epsilon_{l'} - E_{BC}(v_f'). \tag{5}$$

Expanding $V(r,R)$ about the equilibrium value r_0 and retaining only the linear terms in $(r - r_0)$, BJ separated the golden rule expression (4) into an intramolecular term (A) and an intermolecular term (B):[30]

$$\Gamma = \pi AB, \tag{6}$$

with

$$A = |\langle v_i'|r - r_0|v_f'\rangle|^2 \tag{7}$$

and

$$B = \left|\langle l'|\left(\frac{\partial U}{\partial Q}\right)_{r_0}|\epsilon'\rangle\right|^2. \tag{8}$$

For a harmonic B–C potential, the intermolecular term does not depend on the quantum number v_i' since the recoil energy is the same in all v_i' states. The v' dependence of Γ arises from A being proportional to v_i'. From the properties of the operator r, the propensity rule $\Delta v = -1$ follows from Eq. (7). Even for an anharmonic potential the propensity rule is valid to a first-order approximation,[30] and the A term is proportional to v_i' as long as $v_i' < K_{BC}$, where

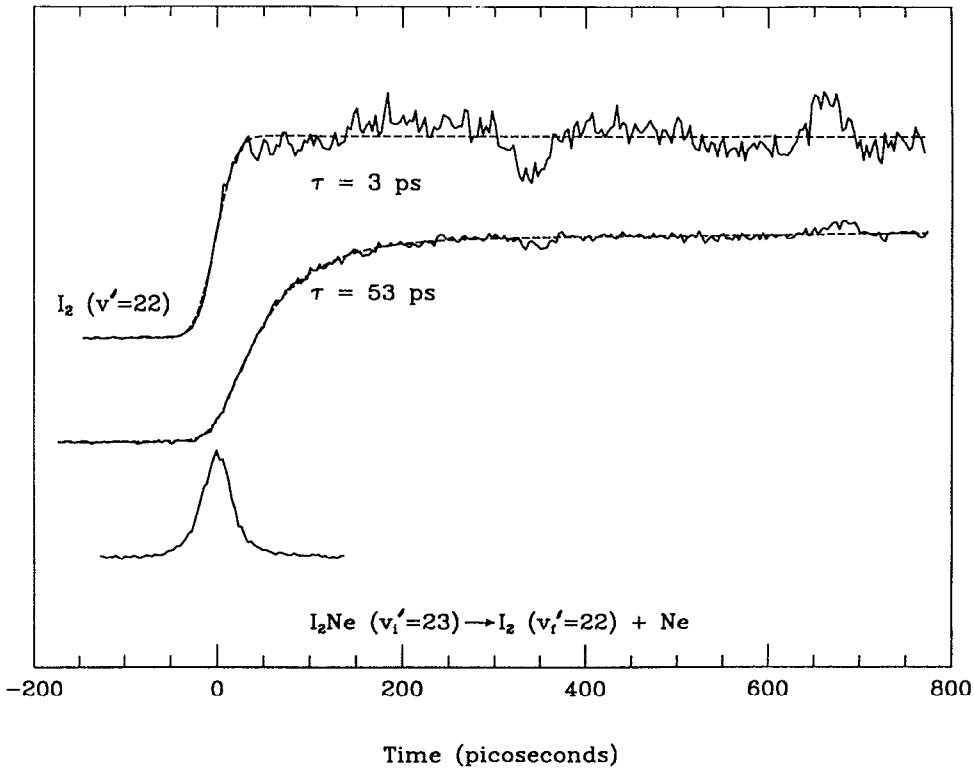

FIG. 7. Shown is a typical transient obtained for the $v_i' = 23/v_f' = 22$ experiments: (top) is a bare I_2 transient obtained for calibration ($v_i' = 22$); (middle) is a transient showing the predissociation ($\tau = 53$ ps); and (bottom) the visible cross correlation of the pump and probe lasers. The dashed line shows a fit to an exponential rise function. For the bare iodine transients, these fits yield a very fast rise as determined by the laser pulse width. The rotational recurrences (cp. Ref. 58) appearing on the "predissociation transient" are those of product I_2 in the $v_f' = 22$ state and match the one for the bare I_2 transient.

$$K_{BC} = \omega_{BC}/[2(\omega x_e)_{BC}]. \tag{9}$$

Here, ω_{BC} is the intramolecular vibrational frequency and $(\omega x_e)_{BC}$ is the corresponding anharmonicity. As BJ pointed out,[30] K_{BC} is large (82.2 for I_2), so for most experiments the above relations are fulfilled.

For a linear X.....B–C bound by a Morse potential,[30]

$$U(Q) = D_{XB}\{\exp[-2\alpha_{XB}(Q-Q_0)] - 2\exp[-\alpha_{XB}(Q-Q_0)]\}, \tag{10}$$

where the distance between B and X is denoted by Q and its equilibrium value by Q_0 (note that Q is different from, but related to, R). The key parameters and relations needed in describing the physics of the problem are given in Table II (see Ref. 30).

For a linear geometry, BJ derived an analytical formula for the VP rate [diabatic distorted wave (DDW) approach]. In the limit $\theta_{\epsilon'} \gg 1$ and taking $v_f' = v_i' - 1$, they obtained

$$\Gamma = \pi^2\hbar\omega_{BC}\mu g(N,l') \times \frac{(2K_{BC} - 2v_i' + 1)(2K_{BC} - 2v_i' - 1)}{[2K_{BC}(2K_{BC} - v_i')]} \times \theta_{\epsilon'}{}^{2N-1} v_i' \exp(-\pi\theta_{\epsilon'}), \tag{11}$$

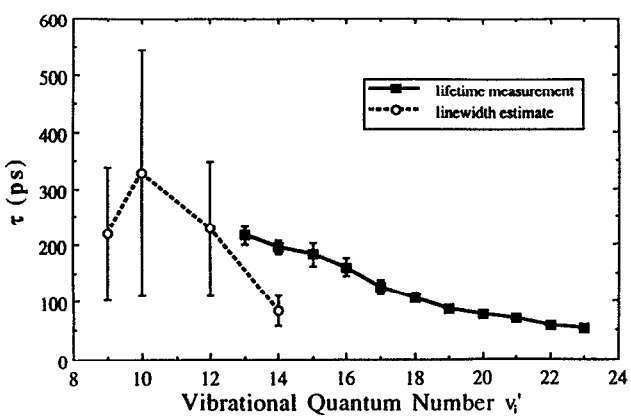

FIG. 8. The vibrational predissociation lifetimes obtained from real-time studies in the present work (labeled by squares and a solid line), and the lifetimes estimated from linewidth measurements by Levy and co-workers given in Ref. 22 (labeled by circles and a dashed line).

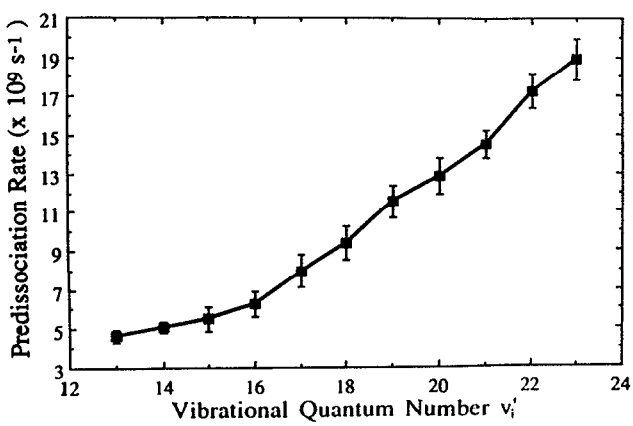

FIG. 9. The rate of vibrational predissociation as a function of the vibrational level v_i' excited.

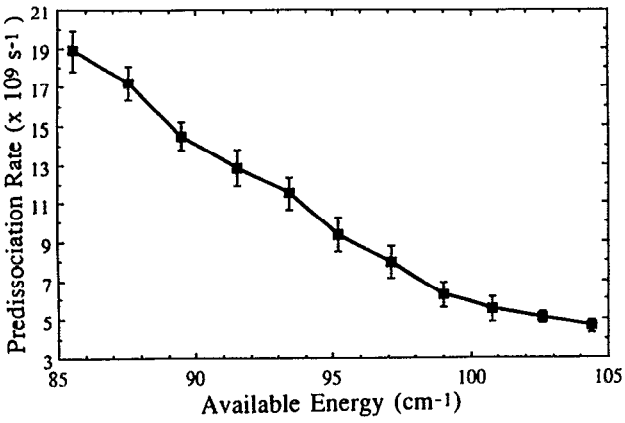

FIG. 10. The rate of vibrational predissociation as a function of the available energy. The available energy is defined as the difference in energy between the v_i' and $v_i' - 1$ vibrational levels of the B-electronic state of I_2. To obtain the translational energy from the available energy one must subtract the vdW binding energy and the internal excitation energy of the fragment I_2^*.

where μ is the mass ratio $\mu_{X,BC}/\mu_{BC}$ and $g(N,l') = (N - l' - 1)/[l'!(2N - l' - 1)!]$.

From this expression some simple physically intuitive relations can be derived. For large values of θ_ϵ, the exponential in expression (11) is dominant, yielding:

$$\Gamma \propto \exp[-\pi(2\mu_{X,BC}\epsilon')^{1/2}/(\hbar\alpha_{XB})], \tag{12a}$$

or equivalently,

$$\Gamma \propto \exp[-2\pi(D_{XB}\epsilon')^{1/2}/(\hbar\omega_{XB})]. \tag{12b}$$

Energy conservation in Eq. (5) leads to

$$\epsilon' = [(\hbar\omega_{BC})(1 - v_i'/K_{BC})] - [D_{XB} - (\hbar^2\alpha_{XB}^2)(K_{XB} - l' - \tfrac{1}{2})^2/(2\mu_{X,BC})], \tag{13}$$

where the first term in square brackets corresponds to the energy difference between the initial and the final state of the I_2 intramolecular vibration, while the second term is the energy of the excited van der Waals vibration with respect to D_{XB}.

From expressions (12) and (13) it can be seen that as the energy difference between levels v_i' and v_f' matches the van der Waals stretch energy of level l' (i.e., $\epsilon' \to 0$), Γ increases. This relation is referred to as the energy-gap law. It also explains why the VP rates are so dependent on the nature of the diatomic B–C in the complex. Equation (12) also reveals the momentum-gap law obtained by Ewing.[34–37] Because the translational momentum p is given by

$$p = (2\mu_{X,BC}\epsilon')^{1/2}, \tag{14}$$

Eq. (12) may be rewritten as

$$\Gamma \propto \exp[-\pi p/(\hbar\alpha_{XB})]. \tag{15}$$

It is now possible to obtain an expression giving the dependence of the VP rate on the vibrational quantum number v_i'. If the second term on the right-hand side of Eq. (13) approaches zero, we can write

$$(D_{XB}\epsilon')^{1/2} = [D_{XB}(\hbar\omega_{BC})]^{1/2}(1 - v_i'/K_{BC})^{1/2} = [D_{XB}(\hbar\omega_{BC})]^{1/2}[1 - v_i'/(2K_{BC})]. \tag{16}$$

In this case, the VP rate, including the intramolecular factor v_i' [according to the A term of equation (6) which is obtained from equation (11) when $K_{BC} \gg v_i'$], leads to

$$\Gamma \propto v_i' \exp(\gamma v_i'), \tag{17}$$

where

$$\gamma = \pi[D_{XB}(\hbar\omega_{BC})]^{1/2}/[K_{BC}(\hbar\omega_{XB})] = \pi[\mu_{X,BC}(\hbar\omega_{BC}/2)]^{1/2}/[K_{BC}(\hbar\alpha_{XB})]. \tag{18}$$

The derivation of Eq. (17) should, however, fail if the energy $\epsilon_{l'}$ cannot be neglected relative to the energy difference between levels v_i' and v_f'. In other words, if the energy difference

TABLE II. Some key parameters and definitions (for Morse potential) used in the theoretical analysis.

D_{XB}	Potential well depth
$\omega_{XB} = \left(\frac{1}{\mu_{X,BC}}\left(\frac{\partial^2 U}{\partial Q^2}\right)_{Q_e}\right)^{1/2}$	Characteristic Morse frequency
$\mu_{X,BC} = \frac{m_X(m_B + m_C)}{(m_X + m_B + m_C)}$	Reduced mass of the complex
$\alpha_{XB} = \omega_{XB}\left(\frac{\mu_{X,BC}}{2D_{XB}}\right)^{1/2}$	Characteristic inverse length[a]
$\epsilon_{l'} = -D_{XB} + h\omega_{XB}\left(l' + \frac{1}{2}\right)\left(1 - \frac{(l' + \frac{1}{2})}{2K_{XB}}\right)$	Energy of the bound state $\lvert l'\rangle$
$\theta_\epsilon = \frac{(2\mu_{X,BC}\epsilon')^{1/2}}{h\alpha_{XB}}$	Energy parameter
$K_{XB} = \frac{2D_{XB}}{h\omega_{XB}}$	Anharmonicity
$N = (K_{XB} + \frac{1}{2})$	Number of bound states in the Morse potential[b]
$\mu_{BC} = \frac{m_B m_C}{(m_B + m_C)}$	Reduced mass of B–C

[a] The relationship between α_{XB} and ω_{XB} is obtained by explicitly considering $\partial^2 U/\partial Q^2$ from Eq. (10).

[b] The value obtained for N in this expression needs to be rounded off to an integer value.

of v_i' and v_f' is much larger than the bound van der Waals level energy, then expression (17) is valid, and we only have the intramolecular effect (v_f' of the pre-exponential A term) and a simple exponential. Γ should show a nonlinear dependence on the quantum number v_i' due to the anharmonicity of the B–C bond, even if ϵ_i' is included.

Within a semiclassical approach,[38] Eq. (17) can be derived. The intermolecular term is approximated by a "free–free" transition between different states of the relative motion of the two fragments. In this semiclassical approach it is assumed that the repulsive part of the potential is responsible for the energy exchange between the fragments. This assumption is essentially in line with a highly excited van der Waals state of the complex, i.e., neglecting the potential well. The half-collision can then be related to a full collision, and the length parameter L mentioned in the introduction is a key parameter to the early time dynamics.

Recently, simple expressions for VP rates, like the momentum-gap law, have been critically reviewed.[39] The authors performed model calculations which showed that the momentum-gap law can lead to severe failure when sufficiently high quantum numbers v_i' are involved.

The D_0 value of the I_2Ne van der Waals bond has been measured to be approximately 65–67 cm^{-1} (Ref. 21), while the available energy for dissociation varies between 104.4 cm^{-1} for $v_i' = 13$, and 85.6 cm^{-1} for $v_i' = 23$. Therefore, for the values of v_i' studied in this experiment, the amount of excess energy going into the fragmentation process is between 19 and 37 cm^{-1}, assuming $l' = 0$.

1. Absolute rate values

Before applying the above-mentioned results to the system I_2Ne a note concerning the approximation is in order. Equation (11), from which the functions important to the VP of I_2Ne are derived, is valid for a cluster geometry assuming a linearized Morse potential in the limit $\theta_{\epsilon'} \gg 1$. With values obtained spectroscopically by Levy and co-workers[21] for the B state of I_2Ne ($\alpha = 1.5$ Å^{-1}, $K_{XB} = 6.21$, $D_{0,XB} = 66.05$ cm^{-1}) and the experimental parameters for the I_2 B state, we obtained $\theta_{\epsilon'} = 3.55$ for $v_i' = 20$. This value for $\theta_{\epsilon'}$ is larger than 1, but it is not a factor of 10 or 100 larger than 1. This may influence the validity limit for using Eq. (11) for the I_2Ne case.

Calculating the VP rate for $v_i' = 20$ according to the more exact equation (2.B.53) in Ref. 30(b) [from which Eq. (11) was derived in the limit $\theta_{\epsilon'} \gg 1$] yields $\tau = 2.7$ ps, a value much too small when compared to our real-time result of 78 ps. With the same parameters one can calculate the VP rate by means of Eq. (11) and end up with $\tau = 2.8$ ns, a value much too large. Other calculations for nonlinear geometries and close couplings are discussed below (Secs. III B 3 and III B 4). Although both equations do not lead to quantitative agreement with our experimental results we feel that fits of the data to these functional forms may be, at least qualitatively, meaningful. The energy-gap law and the momentum-gap law have been applied before in the interpretation of VP processes (see, e.g., Ref. 56) and it is important to test the predicted trends with experiments.

2. Momentum-gap law

With the momentum-gap law we fitted the experimental results to an exponential function according to Eq. (15):

$$1/\tau \propto \exp(\beta\epsilon'^{1/2}). \tag{19}$$

The fit, together with our data, is shown in Fig. 11(a). From the fit parameter β we obtain an effective Morse parameter $\alpha = 3.94$ Å^{-1}. A reasonable value of α should lie in the range 1–2 Å^{-1}. Taking into account the intramolecular term, an attempt to improve equation (19) was made by fitting to the following expression:

$$1/\tau \propto v_i' \exp(\beta\epsilon'^{1/2}). \tag{20}$$

Surprisingly, the fit [Fig. 11(b)] yields a worse value of $\alpha = 6.31$ Å^{-1} Improvement by including the Morse factor [see Eq. (11)],

$$M(v) = (2K_{BC} - 2v + 1) \times (2K_{BC} - 2v - 1)/[2K_{BC}(2K_{BC} - v)], \tag{21}$$

leads to a fit of the type:

$$1/\tau \propto M(v_i')v_i' \exp(\beta\epsilon'^{1/2}), \tag{22}$$

and we obtained a value of $\alpha = 4.89$ Å^{-1}. The fit is shown in Fig. 11(c).

Assuming $l' > 0$, the data could be fitted to the functional form (22) with $\alpha = 4.78$ Å^{-1} ($l' = 1$), $\alpha = 4.10$ Å^{-1}

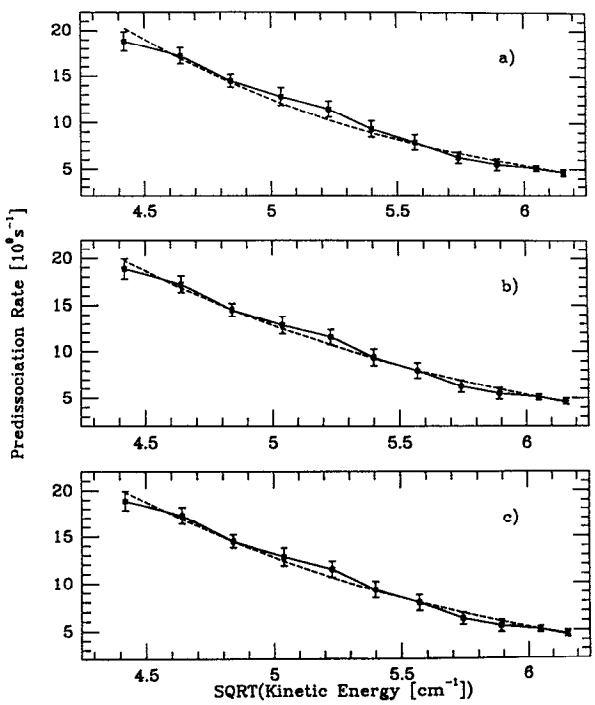

FIG. 11. Theoretical fits of the experimentally determined rates to the models described in the text. The abscissa corresponds to the square root of the kinetic energy of fragmentation with $l' = 0$. The squares given with the error bars represent the data and the dashed lines correspond to a nonlinear least squares fit of these data to functional forms given by: (a) Eq. (19), (b) Eq. (20), (c) Eq. (22). See text for discussions.

($l' = 2$), $\alpha = 3.76$ Å^{-1} ($l' = 3$), $\alpha = 3.56$ Å^{-1} ($l' = 4$); and $\alpha = 3.45$ Å^{-1} if the van der Waals energy $\epsilon_{l'}$ is completely neglected in Eq. (5). Accordingly, higher l' values tend to shift the parameter α to lower values but by no means into the expected range. The functional form suggested by the simple momentum gap law is not sufficient to obtain reasonable Morse parameters from a fit of the experimental data.

Even though Eq. (11) has been derived for triatomic van der Waals clusters in a collinear geometry only, the equation may be used to obtain the following functional form when taking into account the effect of higher terms in $\theta_{\epsilon'}$:

$$1/\tau \propto M(v_i')v_i'(\beta\epsilon'^{1/2})^m \exp(\beta\epsilon'^{1/2}). \quad (23)$$

For $m = 8$ ($l' = 0$) we obtain $\alpha = 1.50$ Å^{-1} and for $m = 9$ ($l' = 0$) $\alpha = 1.38$ Å^{-1}. Similar fits were made but without the intramolecular factor, i.e., to

$$1/\tau \propto (\beta\epsilon'^{1/2})^m \exp(\beta\epsilon'^{1/2}), \quad (24)$$

which yield $\alpha = 1.52$ Å^{-1} for $m = 7$ ($l' = 0$) and $\alpha = 1.40$ Å^{-1} for $m = 8$ ($l' = 0$).

3. Energy-gap law and close coupling

In addition to the momentum-gap law, we next consider the energy-gap law in the limit specified by Eq. (17), i.e.,

$$1/\tau \propto v_i' \exp(\gamma v_i'). \quad (25)$$

From the parameter γ we extract $\alpha = 2.45$ Å^{-1}. The fit is shown in Fig. 12(a). To test the uniqueness of the fit we also attempted a simpler exponential form,

$$1/\tau \propto \exp(\gamma v_i'), \quad (26)$$

which yields $\alpha = 1.53$ Å^{-1} [Fig. 12(b)]. A polynomial fit including linear, quadratic, and cubic terms is shown in Fig. 12(c). From Fig. 12, it is clear that the VP rate shows a definite nonlinear dependence on the vibrational quantum number v_i' as has been predicted by theory, independent of the different functional forms suggested by different limits.

Using the full Morse potential,[30,33] BJ performed numerical model calculations for linear triatomic van der Waals complexes and showed that the results were in line with the qualitative energy-gap law. They found that the dependence of the VP rate on the van der Waals quantum number l' is such that the rate increases with l' up to a maximum and then decreases. If the van der Waals potential can only hold very few (e.g., two) bound states, the rate decreases with l'. BJ also went beyond the golden rule approximation, i.e., included continuum–continuum interactions.[30] Intercontinuum interactions result in relaxing the propensity rule $\Delta v = -1$ and allow different v_f' channels to be open, particularly for high v_i' quantum numbers.

The geometry of I_2Ne is most likely T-shaped,[19] and the influence of any anisotropy in the potential, including effects of the bending motions and rotation, on the rates has not been dealt with here. Hence, α can only be looked upon as an effective parameter. In order to calculate VP rates for nonlinear geometries, numerical techniques have to be invoked as analytical solutions do not exist for this type of problem.

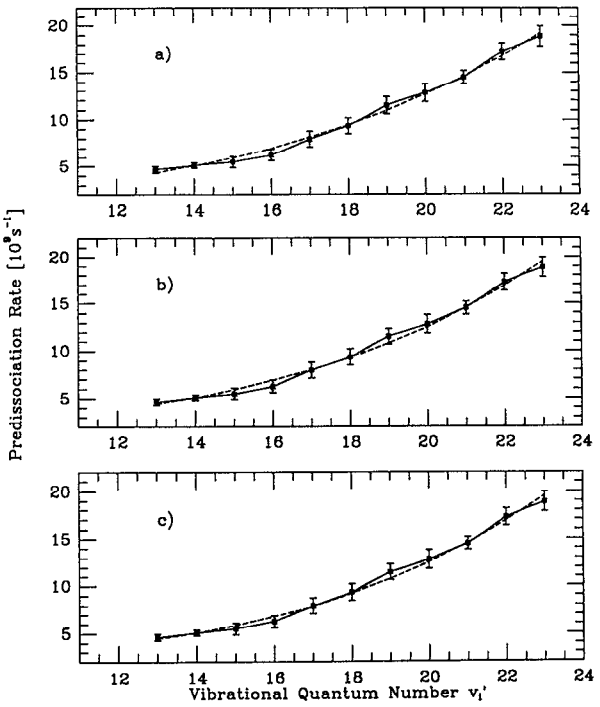

FIG. 12. Theoretical fits of the experimentally determined rates to test the dependencies of these rates on v_i'. The abscissa corresponds to the initially excited vibrational state v_i' of the I_2 moiety. The squares given with error bars represent the experimental data, while the dashed lines correspond to nonlinear least-squares fits of these data to functional forms given by: (a) Eq. (25), (b) Eq. (26), (c) a polynomial including linear, quadratic, and cubic terms. See text for discussions.

BJ solved the close coupling (CC) equations numerically employing the scattering formalism.[31,32] The quasibound states of the complex manifest themselves as scattering resonances, close to the zero-order energies of the bound states of the v'-state-averaged van der Waals potential. The width of these resonances can be related to the rate of VP. Calculations of the VP rates for T-shaped I_2He within this scheme resulted in lowering the rates with respect to analogous calculations in the collinear geometry. The van der Waals potential for the T-shaped complex was taken as a sum of two identical Morse potentials between each I atom and He, where D_{XB} (collinear) $= 2D_{XB}$ (T-shape).[31,32]

The CC calculations for I_2Ne in a collinear configuration were obtained and gave a VP lifetime of about 2 ns for $v_i' = 2$. The parameters used were $\alpha_{XB} = 1.31$ Å^{-1} and $D_{XB} = 100\,\text{cm}^{-1}$. It is difficult to compare this number with our results as the lowest vibrational state covered in our studies is $v_i' = 13$. DDW calculations using the same parameter set led to comparable results. From Fig. 11(b) of Ref. 30a, where some results of VP rate calculations for I_2Ne (collinear geometry) in the DDW framework (including continuum–continuum coupling) were plotted, we can extract some data for, e.g., $v_i' = 20$. With $D_{XB} = 100\,\text{cm}^{-1}$ and $\omega_{XB} = 25\,\text{cm}^{-1}$, the authors obtained a lifetime τ of about 3.5 ps for this vibrational quantum number; changing ω_{XB} to $20\,\text{cm}^{-1}$ leads to about 5 ps, and with $D_{XB} = 95\,\text{cm}^{-1}$ and $\omega_{XB} = 35\,\text{cm}^{-1}$ they obtained ca. 500 fs. These calculations

were performed by choosing l' to be the van der Waals stretch quantum number that maximizes the VP rate. All of the above calculations do not agree with the absolute magnitudes obtained experimentally (see Table I).

4. Effect of rotations, and other models

In order to take into account the effect of rotational excitation, calculations within the rotational infinite order sudden approximation (RIOSA) have been performed for I_2X complexes.[40,41] As the rotational energies are smaller than the vibrational stretching energies, the rotations are treated adiabatically. Vibrational–rotational coupling as well as centrifugal coupling can also be included. RIOSA calculations have been performed in the Fermi golden rule diabatic distorted wave framework, and in the CC framework where the CC equations are solved exactly for each angle θ and the rotationally averaged resonance widths yield the desired VP rates.[41] Calculations on I_2He show that the effect of the rotations on the excitation is negligible (pure V–T process) and on the VP rates leads to a further slowing down with respect to the T-shaped geometry.[30,41]

An interesting result emerges from these calculations. By going from the linear configuration to the T-shaped configuration and including rotations, the additional degree of freedom seems to stabilize the complex with respect to VP.[30b]

Delgado-Barrio and co-workers performed three-dimensional CC RIOSA type calculations in order to obtain VP rates for I_2Ne.[42] For $v_i' = 28$ ($l' = 0$, no van der Waals bending excitation) they calculated VP rates for different angles θ. Their angle-averaged VP rate leads to a lifetime of about 13 ps which is in line with our results ($v_i' = 23$: 53 ps) as the rate is expected to increase nonlinearly with v_i'. The parameters these authors used[43] were $D_{XB} = 66.48\ cm^{-1}$ and $\alpha_{XB} = 1.9\ Å^{-1}$.

Further improvements of the above described procedures have been proposed. An adiabatic distorted wave (ADW) approach, by Halberstadt and Beswick,[44] and an adiabatic model including non-Condon effects, by Kokubo and Fujimura,[45] have been formulated. There are other calculations on different van der Waals molecules (see, e.g., Refs. 46–48).

The adiabatic calculation by Kokubo and Fujimura[45] of the VP rate of I_2Ne employed the parameters $D_{XB} = 94.7\ cm^{-1}$ and $\alpha_{XB} = 1.38\ Å^{-1}$. They chose a collinear geometry for the complex. From Fig. 4 of their paper we extract a lifetime of ca. 15 ps ($v_i' = 20$, $l' = 2$) in the Condon approximation, a value which should be compared with our result of 78 ps for the same level. Inclusion of non-Condon effects, however, led Kokubo and Fujimura to a lifetime of about 650 fs, which is far too small even if one considers that they did not perform calculations for $l' = 0$.

Schatz, Gerber, and Ratner introduced a SCF Hartree product as an initial state into the DDW calculations.[49] They performed calculations on the VP of I_2Ne in a collinear geometry. With the same parameters as BJ they obtained very good agreement with the DDW calculations including continuum–continuum interactions.[30]

5. Classical trajectory and RRKM calculations

Classical trajectory calculations have been performed by several groups[41,50–52] on I_2He, I_2Ar, and on I_2Ne above $v_i' = 35$ (in the crossover range were the $v_i' - 1$ channel closes).[41,53] The results agree quite well with quantum calculations. Unfortunately, to our knowledge, there does not exist a classical trajectory study on I_2Ne in the range covered by our experiments, but these calculations are now under way in the groups of S. A. Rice[54a] and G. Delgado-Barrio.[54b]

Gray and Rice discussed an alternative RRKM (ARRKM) method, in addition to quantum mechanical and classical dynamical calculations,[52] and performed calculations on I_2Ar (*vide infra*). Very recently a time-dependent wave packet approach[55] has been proposed which will prove particularly useful when we experimentally bridge the femtosecond wave packet dynamics to the picosecond dynamics of VP (this work).

IV. THE I_2Ar SYSTEM

In two ways I_2Ar behaves differently from I_2Ne. First, as the depth of the van der Waals potential ($D_0 = 220$–$226.3\ cm^{-1}$) is much larger than that of I_2Ne, the VP process favors the channel $v_f' = v_i' - 3$ (see Ref. 22). Second, VP in I_2Ar is accompanied by a competing electronic predissociation (EP), as reported by Levy and co-workers[22] and by Atkinson and co-workers.[57] Thus, the measured rates are expected to be faster than those determined by pure VP, which is one of the two channels describing the dynamics:

$$I_2Ar^*(v_i') \xrightarrow{k_{vp}} I_2^*(v_f' = v_i' - 3) + Ar \tag{27a}$$

$$\xrightarrow{k_e} I + I + Ar. \tag{27b}$$

For the I_2Ar experiments reported here, the pump laser excites the complex into a vibrational level v_i'. The probe laser detects the nascent I_2^* in its B-state vibrational level $v_f' = v_i' - 3$ by exciting it to an I_2 ion pair state from which fluorescence was collected. The transients measured for $v_i' = 21$, $v_f' = 18$ and for $v_i' = 18$, $v_f' = 15$, together with the corresponding bare iodine transients $v' = 18$ and $v' = 15$, are shown in Figs. 13(a) and 13(b), respectively. From least-squares fits to the exponential rise we obtained a rise time of 77 ± 8 ps for $v_i' = 21$ and 70 ± 11 ps for $v_i' = 18$. An estimate of 30 ps for $v_i' = 15$ was obtained from linewidth measurements;[22] the spectral bands are inhomogeneously broadened due to unresolved rotational bands.

A. VP and EP rates

Evidence for non-negligible EP in I_2Ar comes from measurements of the fluorescence intensity of I_2^*, formed after excitation of the complex, as a function of v_i'. Levy and co-workers found strong "oscillations" which were not exhibited by the complexes I_2He and I_2Ne.[22] Using intracavity absorption, fluorescence quantum yield studies, by Atkinson and co-workers,[57] showed such oscillations. These

oscillations were attributed to variations in k_e with v_i', presumably caused by the crossing of the B state with the repulsive Π state(s).

From our experiments we obtain the absolute state-to-state rate for $v_i' = 21$ and for $v_i' = 18$, and we may use these rates and a simple kinetic scheme to obtain the ratio of the VP rate constants $k_{vp}(v_i' = 21)/k_{vp}(v_i' = 18)$. The model features the following channels:

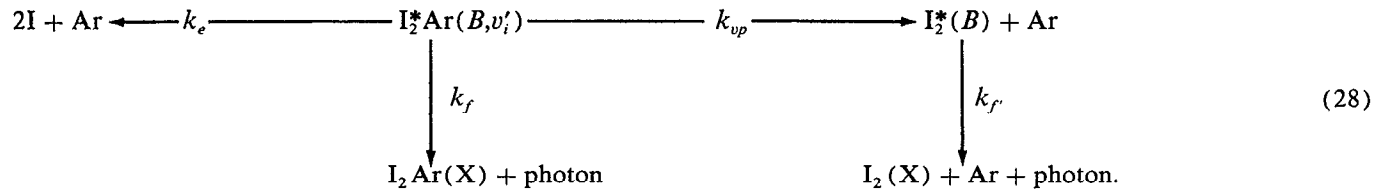

(28)

Assuming $k_f, k_{f'} \ll k_{vp}, k_e$, the number of I_2^* molecules can be expressed as

$$[I_2^*](t) = N_0 k_{vp}/(k_{vp} + k_e)\{1 - \exp[-(k_{vp} + k_e)t]\}, \tag{29}$$

where N_0 denotes the number of initially ($t = 0$) excited I_2Ar^* (v_i') complexes. The final number of nascent I_2^* is formed before any appreciable radiative decay, and thus,

$$[I_2^*]_\infty = N_0 k_{vp}/(k_{vp} + k_e), \tag{30}$$

which also corresponds to the number of photons emitted (μs time scale) if only the radiative decay of I_2^* is assumed. In order to obtain an expression for the normalized fluorescence,[22] we have to consider the excitation of bare iodine into the vibrational level v_i'. Exciting N_0' of I_2 molecules into v_i' leads to a collection of N_0' fluorescence photons if the fluorescence quantum yield is one. The normalized fluorescence can then be expressed as follows:

$$F(v_i') = k_{vp}(v_i')/[k_{vp}(v_i') + k_e(v_i')][N_0(v_i')/N_0'(v_i')]. \tag{31}$$

From the state-to-state real-time measurements, the rise time gives

$$\tau(v_i') = [k_{vp}(v_i') + k_e(v_i')]^{-1}, \tag{32}$$

which when combined with Eq. (31) yields the ratio of interest,

$$F(21)/F(18) = N_0(21)N_0'(18)/[N_0(18)N_0'(21)] * [\tau(21)/\tau(18)][k_{vp}(21)/k_{vp}(18)]. \tag{33}$$

Assuming that the relevant Franck–Condon factors of bare I_2 and I_2 within the complex do not differ significantly (i.e., the presence of the Ar atom does not disturb the shape and equilibrium position of the potential curves for absorption), and, furthermore, assuming that the experimental conditions under which the complex spectra were measured and those under which the bare iodine experiments were performed are identical, Eq. (33) reduces to

$$k_{vp}(21)/k_{vp}(18) = [F(21)/F(18)][\tau(18)/\tau(21)]. \tag{34}$$

This equation relates the state-to-state rates to the ratio of the VP rate constants. $F(21)/F(18) = 3$, as estimated from Fig. 2 of Ref. 22, and our real-time results, when used in Eq. (34), give a ratio $k_{vp}(21)/k_{vp}(18)$ of about 2.9. Accordingly, k_{vp} increases with increasing the quantum number v_i' whereas k_e increases with decreasing v_i'. This latter behavior may be the reason why I_2Ar complexes have not been observed for low v_i', and is consistent with the quantum yield results obtained by Atkinson and co-workers.[57]

B. Calculations of the VP rates and their v_i' dependence

Exploring the effect of the anharmonicity of the intramolecular bond on the behavior of the VP rate as a function of v_i', BJ presented some calculations for I_2Ar (collinear geometry) in Table I of Ref. 33. From these data we obtain the ratio $k_{vp}(20)/k_{vp}(15) = 5.6$. Assuming a v^6 dependence in this region ($20^6/15^6 = 5.6$) we arrive at $k_{vp}(21)/k_{vp}(18) = 2.5$, which is in good agreement with the finding of 2.9 reported here. Furthermore, in Ref. 30b, BJ quoted a private communication with D. H. Levy who deduced a v^5 dependence of k_{vp} (unpublished). Such a dependence leads to a ratio $k_{vp}(21)/k_{vp}(18) = 2.2$ which is still in fair agreement with our result.

As in the case of I_2Ne, the VP rate of I_2Ar increases with increasing v_i', in accord with theory. However, the absolute magnitudes calculated for the VP rates are not in very good agreement with our results and vary significantly with the assumed parameters of the van der Waals potential. These calculations do not account for EP.

Using the values $D_{XB} = 200$ cm^{-1} and $\alpha_{XB} = 1.25$ Å^{-1}, BJ predicted a VP lifetime of about 25 ps for $v_i' = 20$ (collinear geometry).[30] Changing α to 2.02 Å^{-1} led to $\tau(2) < 10$ ps[31] which is far too small; for $v_i' = 21$ the calculated VP time is thus expected to be shorter than 10 ps by orders of magnitude. DDW, ADW, and CC calculations yielded comparable results.[44] Calculations of VP of I_2Ar in a nonlinear geometry have, to our knowledge, not yet been performed. According to the results obtained for I_2He (*vide supra*), calculations for a T-shaped geometry, and especially three-dimensional calculations, are expected to lead to a de-

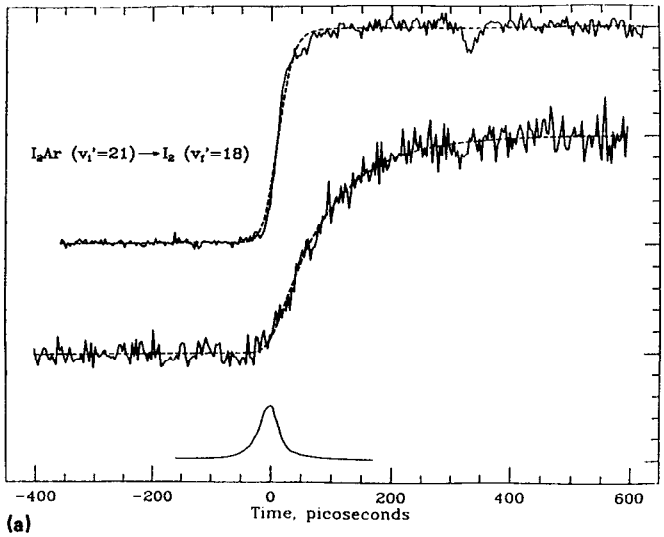

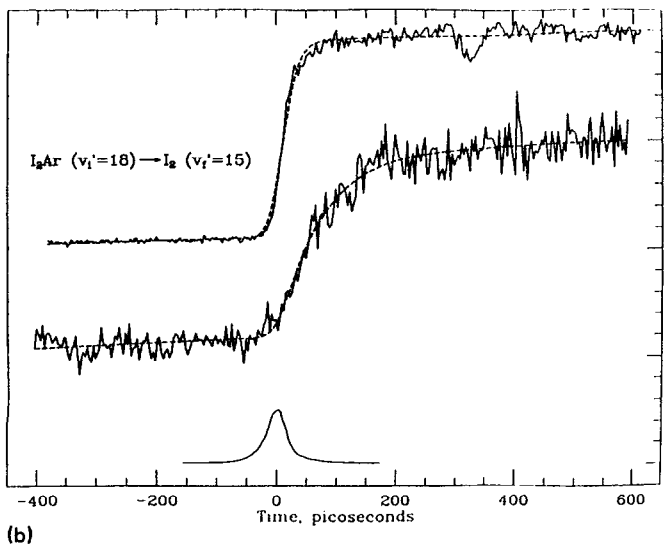

FIG. 13. (a) Transients of the I_2Ar system displaying the build-up and the measurement of state-to-state rates. Shown is a typical transient obtained for the $v_i' = 21/v_f' = 18$ experiments; (top) is a bare I_2 transient obtained for calibration ($v' = 18$). Rotational recurrences (see text) are evident; (middle) is the transient showing the predissociation process; and (bottom) the visible cross correlation of the pump and probe lasers. The dashed lines show fits to an exponential rise function. For the bare iodine transients, the fit yields a very fast rise, as determined by the cross correlation. (b) Same as Fig. 13(a), but for $v_i' = 18/v_f' = 15$ predissociation; the bare I_2 transient is that for ($v_i' = 15$). See text for details.

crease of the VP rates. This trend would then shift the results into the right direction for bridging the gap between theory and experiments.

Gray and Rice[52] performed classical dynamics (CD), Fermi golden rule (FGR), and ARRKM calculations in order to obtain the VP rates of I_2Ar in its B state. They used the same parameters as BJ in Ref. 30(a) and for $v_i' = 2$ they obtained VP times of about 6 ps (CD), 8 ps (FGR), and 4.5 ps (ARRKM). These numbers are consistent despite the differences between the various models but still appear far too small in comparison with our experimental data. Correcting for the effect of van der Waals stretch excitation (quantum number l') can help the results by only about an order of magnitude, which is not sufficient for quantitative agreement (note that our experiments were performed for $v_i' = 18,21$).

From Fig. 4 of the publication by Kokubo and Fujimura,[45] who applied their adiabatic scheme to the VP of I_2Ar (collinear geometry), we extract VP times of about 26 ps ($v_i' = 21, l' = 13$), and 11 ps ($v_i' = 21, l' = 8$) in the Condon approximation, and of about 4 ps ($v_i' = 21, l' = 13$), and 1.3 ps ($v_i' = 21$, $l' = 8$) when non-Condon effects are accounted for. From the same figure, we deduce VP times of about 53 ps ($v_i' = 18, l' = 13$), and 21 ps ($v_i' = 18, l' = 8$) in the Condon approximation, and of about 9.5 ps ($v_i' = 18$, $l' = 13$), and 2.7 ps ($v_i' = 18$, $l' = 8$) after including non-Condon effects (it would be very interesting to obtain results for $l' = 0$ in this scheme). Clearly, the inclusion of non-Condon effects seems to shorten the lifetimes tremendeously, and this appears to be a trend in the wrong direction as noted in the case of I_2Ne discussed above.

V. CONCLUSIONS

In this paper we have presented the results of our real-time studies of vibrational predissociation (VP) in I_2X clusters, where X = Ne, and Ar. State-to-state rates were measured, and the results were compared with a number of theoretical findings. These experiments were performed using a combination of time-resolved (pump–probe) picosecond laser spectroscopy and molecular beam techniques. A detailed description of the experimental apparatus used in these studies was presented.

The experimentally determined rates in real-time differ from those obtained by linewidth measurements due to the inhomogeneous and other broadening channels, as discussed above. The state-to-state rates of VP showed a nonlinear dependence (increase) on v_i', or, an inverse dependence (decrease) on the energy available for VP over the range of v_i' studied. This nonlinear behavior is in qualitative agreement with a number of theoretical models proposed for VP in these systems and detailed here for comparisons with our experimental results. The theoretical models, however, do not yet provide accurate and unique absolute values of the state-to-state rates, although they appear to be in agreement with each other. For quantitative comparisons with experiments, theory must address the 3-D dynamical aspect (bending, etc.) of the problem and the nature of the potential. There are, however, some simple descriptions that emerge.

The overall change of the rates with v_i' can be understood using a simple semiclassical model of full-collision theory. In this model the translational energy is transferred to a vibrational energy, and the reverse case can be considered for the "half-collision" VP process. In the half-collision, the repulsion occurs in a few hundreds of femtoseconds and nonadiabatic energy transfer is expected since the vibrational period is ~300 fs. The energy flow of the I_2 vibrational exci-

tation to the I_2–Ne coordinate is the bottleneck since, in a kinematic description, the time for bond breakage (at the translational energy of interest) is ~ 1 ps and the inverse rates are typically 50–200 ps.

The time scale for rotations is different from both the impulsive dissociation time and the inverse rate times. For example, in $v_f' = 20$ the rotational period is 660 ps for $J = 1$ and 66 ps for $J = 10$. Thus, if VP is fast compared with rotations, the rotational alignment of nascent I_2^* in the dissociation of I_2Ne^* will be preserved and rotational recurrences become observable. Analysis of these recurrences gives both the rotational constant of the nascent fragment (i.e., identification of v_f') and the nascent rotational temperature.[58] As discussed in the text, the observations are also relevant to the theoretical treatment of the effect of rotations on VP. Elsewhere, we have reported details of the theory[59] and applications[60] to dissociation reactions.

For I_2Ar the above simple picture of VP may still apply, but the problem of breaking the I–I bond in the presence of Ar (the so called electronic predissociation, EP) is far from being completely understood. The rate measurements indicate that both VP and EP are comparable in magnitude and that VP increases with v_i' while EP decreases with increasing v_i'. The simplest explanation is that the Ar couples the B-state surface to a repulsive surface (e.g., $^1\Pi_{1u}$). The problem becomes Landau–Zener type dynamics with the avoided crossing determining the overall rate of forming I + I, as in the case of NaI.[61] This nonadiabatic coupling between the B state and the repulsive state may be enhanced by Ar due to spin-orbital coupling and the break-down of the Born–Oppenheimer approximation (in I_2 alone there is a weak electronic predissociation caused by hyperfine interactions[62]).

This type of nonadiabatic coupling scheme between the repulsive state (excited above the I + I* dissociation limit) and the B state (the reverse of the above discussed case) has been proposed[63] for another interesting problem. When I_2Ar is excited above the I + I* dissociation limit, it produces fluorescence from the bound levels of the B state.[64] The Ar-induced coupling[65] mixes the repulsive potential and the B-state potential and thus some fluorescence is expected. It is also possible that the entire dynamics do not involve the repulsive surface, and that the I_2 is "caged"[64] by an Ar atom. As a result of a possible charge transfer type interaction it may be that Ar electrons promote an antibonding I_2 excitation similar to known bimolecular reactions involving I_2. To address these and other questions we hope to be able to follow the dynamics from the fs (preparation) to the ps (dissociation) time domain to study the early time signature of the wave packet motion. There are other interesting systems, studied by the Janda group[66] and the Lester group,[10,56(c)] that these real-time experiments should be extended to, hopefully to relate the nature of (different) bonding to the dynamics.

This paper is the first in a series focusing on the dynamics of small clusters. In a future publication,[16] studies of the larger clusters, I_2Ne_n (where $n > 1$), will be presented. These larger clusters, with their "controlled" increased degrees of freedom, offer an opportunity for understanding the dynamics of IVR, relaxation, and dissociation in finite-sized systems. As with I_2Ne and I_2Ar, direct theoretical and experimental comparisons will be made. With fs time resolution we should be able to observe the coherent dynamics of the I_2X_n systems and make comparison with the wave packet dynamics of I_2.[14]

ACKNOWLEDGMENTS

This work was supported by a grant from the National Science Foundation (DMR). L. W. Peng and P. Cong contributed to the construction of the laboratory apparatus described in the earlier communication[27] and in this paper. We are grateful to their help and the many discussions we had with them. We have also enjoyed discussions with Professor E. E. Nikitin and Professor J. A. Beswick during their visits to Caltech, and with Professor G. Delgado-Barrio on some

[1] A. D. Buckingham, P. W. Fowler, and J. M. Hutson, Chem. Rev. **88**, 963 (1988)
[2] K. I. Peterson, G. T. Fraser, D. D. Nelson, and W. Klemperer, in *Comparison of Ab Initio Quantum Chemistry with Experiments for Small Molecules: The State of the Art*, edited by R. J. Bartlett (Reidel, Dordrecht, 1985), p. 217.
[3] L. Khundkar and A. H. Zewail, Annu. Rev. Phys. Chem. **41**, 15 (1990), and references therein.
[4] (a) J. J. F. Ramaekers, H. K. van Dijk, J. Langelaar, and R. P. H. Rettschnick, Faraday Discuss. Chem. Soc. **75**, 183 (1983); (b) M. Heppener, A. G. M. Kunst, D. Bebelaar, and R. P. H. Rettschnick, J. Chem. Phys. **83**, 5341 (1985).
[5] P. M. Weber and S. A. Rice, J. Chem. Phys. **88**, 6120 (1988).
[6] S. A. Wittmeyer, A. J. Kaziska, A. L. Hotyka, and M. R. Topp, Chem. Phys. Lett. **154**, 1 (1989).
[7] D. M. Semmes, J. S. Baskin, and A. H. Zewail, J. Chem. Phys. **92**, 3359 (1990).
[8] M. R. Nimlos, M. A. Young, E. R. Bernstein, and D. F. Kelley, J. Chem. Phys. **91**, 5268 (1989).
[9] (a) M. P. Cassassa, J. C. Stephenson, and D. S. King, J. Chem. Phys. **89**, 1966 (1988); (b) M. P. Cassassa, Chem. Rev. **88**, 815 (1988).
[10] (a) J. C. Drobits, J. M. Skene, and M. I. Lester, J. Chem. Phys. **84**, 2896 (1986); (b) J. C. Drobits and M. I. Lester, *ibid.* **86**, 1662 (1987); (c) J. C. Drobits and M. I. Lester, *ibid.* **88**, 120 (1987).
[11] (a) R. E. Miller, J. Phys. Chem. **90**, 3301 (1986); (b)Science **240**, 447 (1988).
[12] (a) K. C. Janda, Adv. Chem. Phys. **60**, 2011 (1985); (b) F. G. Celii and K. C. Janda, Chem. Rev. **86**, 507 (1986); (c). K. C. Janda and C. Bieler, in *Atomic and Molecular Clusters*, edited by E. R. Bernstein (Elsevier, Amsterdam, 1990), p. 455.
[13] W. R. Gentry, in *Structure and Dynamics of Weakly Bound Molecular Complexes*, NATO ASI series, edited by A. Weber (Reidel, Dordrecht, 1987), p. 467.
[14] (a) R. M. Bowman, M. Dantus, and A. H. Zewail, Chem. Phys. Lett. **161**, 297 (1989); (b) M. Dantus, R. M. Bowman, and A. H. Zewail, Nature **343**, 737 (1990); (c) M. Gruebele, G. Roberts, M. Dantus, R. M. Bowman, and A. H. Zewail, Chem. Phys. Lett. **166**, 459 (1990).
[15] J. J. Breen, D. M. Willberg, M. Gutmann, and A. H. Zewail, J. Chem. Phys. **93**, 9180 (1990).
[16] M. Gutmann, D. M. Willberg, and A. H. Zewail (to be published).
[17] D. H. Levy, Adv. Chem. Phys. **47**, part 1, 323 (1981).
[18] W. Sharfin, K. E. Johnson, L. Wharton, and D. H. Levy, J. Chem. Phys. **71**, 1292 (1979).
[19] J. E. Kenny, K. E. Johnson, W. Sharfin, and D. H. Levy, J. Chem. Phys. **72**, 1109 (1980).
[20] K. E. Johnson, W. Sharfin, and D. H. Levy, J. Chem. Phys. **74**, 163 (1981).
[21] J. A. Blazy, B. M. DeKoven, T. D. Russell, and D. H. Levy, J. Chem. Phys. **72**, 2439 (1980).
[22] G. Kubiak, P. S. H. Fitch, L. Wharton, and D. H. Levy, J. Chem. Phys. **68**, 4477 (1978).
[23] R. E. Smalley, L. Wharton, and D. H. Levy, J. Chem. Phys. **68**, 671 (1978).
[24] A. H. Zewail, Acc. Chem Res. **13**, 360 (1980).

[25] For a review on the separations of time (T_1 and T_2) for homogeneously broadened transitions see: M. J. Burns, W. K. Liu, and A. H. Zewail in *Spectroscopy and Excitation Dynamics of Condensed Molecular Systems*, edited by V. M. Agranovich and R. M. Hochstrasser (North Holland, New York, 1983), Vol. IV, p. 301.
[26] See, for example, (a) R. S. Mulliken, J. Chem. Phys. **55**, 288 (1971); (b) S. Gerstenkorn and P. Luc, J. Phys. (Paris) **46**, 867 (1985); (c) J. C. D. Brand and A. R. Hoy, Appl. Spectros. Rev. **23**, 285 (1987).
[27] J. J. Breen, L. W. Peng, D. M. Willberg, A. Heikal, P. Cong, and A. H. Zewail, J. Chem. Phys. **92**, 805 (1990).
[28] (a) This laser is based on a design used in Professor J. Simon's group, which is a modification of a dye laser design described in F. G. Patterson, Ph.D. thesis, Stanford University, 1985, p. 37; (b) J. C. Postlewaite, J. B. Miers, C. C. Reiner, and D. D. Dlott, IEEE J. Quantum Electron. **24**, 411 (1988).
[29] P. R. Bevington, *Data Reduction and Error Analysis for the Physical Sciences* (McGraw-Hill, New York, 1969), p. 204.
[30] (a) J. A. Beswick and J. Jortner, J. Chem. Phys. **68**, 2277, (1978); (b) J. A. Beswick and J. Jortner, Adv. Chem. Phys. **47**, part I, 363 (1981).
[31] J. A. Beswick and J. Jortner, J. Chem. Phys. **69**, 512 (1978).
[32] J. A. Beswick, G. Delgado-Barrio, and J. Jortner, J. Chem. Phys. **70**, 3895 (1979).
[33] J. A. Beswick and J. Jortner, Molec. Phys. **39**, 1137 (1980).
[34] G. E. Ewing, J. Chem. Phys. **71**, 3143 (1979).
[35] G. E. Ewing, J. Chem. Phys. **72**, 2096 (1980).
[36] G. E. Ewing, Farad. Discuss. Chem. Soc. **73**, 325, 402 (1982).
[37] G. E. Ewing, J. Phys. Chem. **90**, 1990 (1986).
[38] Paper in preparation: collaboration between this group and Prof. E. E. Nikitin.
[39] R. J. Le Roy, M. R. Davies, and M. E. Lam, J. Phys. Chem. **95**, 2167 (1991).
[40] G. Delgado-Barrio, P. Villarreal, A. Varade, N. Martin, and A. Garcia, in *Structure and Dynamics of Weakly Bound Molecular Complexes*, NATO ASI series, edited by A. Weber (Reidel, Dordrecht, 1987), p. 573.
[41] G. Delgado-Barrio, "Predissociation in van der Waals Molecules," Lecture Notes for the "Fourth Europhysics Summer School on Chemical Physics: Molecular Dynamics with Lasers," Murcia, Spain (1989).
[42] A. M. Cortina, S. Miret-Artes, P. Villarreal, and G. Delgado-Barrio, J. Mol. Struct. **142**, 513 (1986).
[43] E. de Pablo, S. Miret-Artes, P. Mareca, P. Villarreal, and G. Delgado-Barrio, J. Mol. Struct. **142**, 505 (1986).
[44] N. Halberstadt and J. A. Beswick, Farad. Discuss. Chem. Soc. **73**, 357 (1982).
[45] T. Kokubo and Y. Fujimura, J. Chem. Phys. **85**, 7106 (1986).
[46] B. P. Reid, K. C. Janda, and N. Halberstadt, J. Phys. Chem. **92**, 587 (1988).
[47] O. Roncero, J. A. Beswick, N. Halberstadt, P. Villarreal, and G. Delgado-Barrio, J. Chem. Phys. **92**, 3348 (1990).
Barrio, J. Chem. Phys. **92**, 3348 (1990).
[48] R. L. Waterland, M. I. Lester, and N. Halberstadt, J. Chem. Phys. **92**, 4261 (1990).
[49] G. C. Schatz, R. B. Gerber, and M. A. Ratner, J. Chem. Phys. **88**, 3709 (1988).
[50] J. A. Beswick, G. Delgado-Barrio, P. Villarreal, and P. Mareca, Farad. Discuss. Chem. Soc. **73**, 406 (1982).
[51] G. Delgado-Barrio, P. Villarreal, P. Mareca, and G. Albelda, J. Chem. Phys. **78**, 280 (1983).
[52] S. K. Gray and S. A. Rice, Farad. Discuss. Chem. Soc. **82**, 307 (1986).
[53] G. Delgado-Barrio, P. Villarreal, P. Mareca, and J. A. Beswick, J. Comput. Chem. **5**, 322 (1984).
[54] (a) S. A. Rice (private communication); (b) G. Delgado-Barrio (private communication).
[55] P. Villarreal, S. Miret-Artes, O. Roncero, G. Delgado-Barrio, J. A. Beswick, N. Halberstadt, and R. D. Coalson, J. Chem. Phys. **94**, 4230 (1991).
[56] (a) D. E. Brinza, C. M. Western, D. D. Evard, F. Thommen, B. A. Swartz, and K. C. Janda, J. Phys. Chem. **88**, 2004 (1984); (b) L. J. van de Burgt, J.-P. Nicolai, and M. C. Heaven, *ibid.* **81**, 5514 (1984); (c) M. T. Berry, M. R. Brustein, and M. I. Lester, *ibid.* **92**, 6469 (1990).
[57] N. Goldstein, T. L. Brack, and G. H. Atkinson, J. Chem. Phys. **85**, 2684 (1986).
[58] D. M. Willberg, J. J. Breen, M. Gutmann, and A. H. Zewail, J. Phys. Chem. **95**, 7136 (1991).
[59] A. H. Zewail, J. Chem. Soc., Faraday Trans. 2 **85**, 1221 (1989).
[60] (a) M. Dantus, R. M. Bowman, J. S. Baskin, and A. H. Zewail, Chem. Phys. Lett. **159**, 406 (1989); (b) J. S. Baskin, D. Semmes, and A. H. Zewail, J. Chem. Phys. **85**, 7488 (1986).
[61] (a) T. S. Rose, M. J. Rosker, and A. H. Zewail, J. Chem. Phys. **88**, 6672 (1988); (b) M. J. Rosker, T. S. Rose, and A. H. Zewail, Chem. Phys. Lett. **146**, 175 (1988); (c) T. S. Rose, M. J. Rosker, and A. H. Zewail, J. Chem. Phys. **91**, 7415 (1989).
[62] (a) M. Broyer, J. Vigue, and J.-C. Lehmann, J. Chem. Phys. **64**, 4793 (1976); (b) H. Levebvre-Brion and R. W. Field, *Perturbations in the Spectra of Diatomic Molecules* (Academic, Orlando, FL, 1986).
[63] J. A. Beswick, R. Monot, J.-M. Philippoz, and H. van den Bergh, J. Chem. Phys. **86**, 3965 (1987).
[64] (a) J. J. Valentini and J. B. Cross, J. Chem. Phys. **77**, 572 (1982); (b) J.-M. Philippoz, R. Monot, and H. van den Bergh, *ibid.* **93**, 8676 (1990), and references therein.
[65] The energy was found to drop by $\sim 1000\ \mathrm{cm}^{-1}$ to the bound fluorescing levels. We have calculated that in order for this process to compete with dissociation efficiently, the matrix element for the coupling has to be on the order of $400\ \mathrm{cm}^{-1}$.
[66] C. R. Bieler, K. E. Spence, and K. C. Janda, J. Phys. Chem. **95**, 5058 (1991), and references therein.